SPACE TELESCOPE SCIENCE INSTITUTE
Operated for NASA by AURA

Instrument Science Report WFC3 2015-06

The Impact of Blobs on WFC3/IR Stellar Photometry

M. J. Durbin, P. R. McCullough

April 27, 2015

Abstract

We investigate the impact of the anomalous regions known as "blobs" on WFC3/IR stellar photometry using observations of globular cluster ω Centauri in five commonly used WFC3/IR filters, and test the effectiveness of a "blob flat field" created to negate the effects of blobs. McCullough et al. (2014) claim that the use of a blob flat field will decrease the accuracy of stellar photometry rather than improve it; however, we show here that the application of the blob flat field is effective for improving stellar photometry in blob-affected regions.

keywords: *Hubble Space Telescope, HST - instrumentation: detectors - methods: data analysis - techniques: image processing - Wide Field Camera 3, WFC3/IR*

Introduction

The presence of "blobs" in WFC3 IR channel images was observed shortly after WFC3's installation in 2009, and was first described by Pirzkal, Viana, & Rajan (2010). Blobs are small, roughly circular regions of moderate (up to ∼20%, typically closer to 5 - 10%) attenuation caused by particulate matter on the CSM mirror. McCullough et al. (2014, hereafter

M14) have provided a complete census of all known blobs up to the date of publication, including position, radius, and date of first appearance. They have also created a flat field designed to correct for blob attenuation, and make recommendations for its use. Here we present a quantitative analysis of the impact of blobs on stellar photometry, and the effectiveness of the "blob flat field" in mitigating the effects of blobs.

The blob flat field described by M14 is a 1014×1014 FITS image with a value of unity everywhere except at the locations of blobs, where the values are a measure of the fractional attenuation each pixel within the blob experiences (see M14 for details on the creation of the flat field). M14 warns against using the blob flat field for stellar photometry, reasoning that since the optical cross-sections of the particulates responsible for the blobs are typically smaller than a single IR pixel, it is unlikely that the beam of light from the star will intersect with the particulate at all, and thus dividing stellar images by the blob flat field will erroneously increase the measured stellar flux.

Photometry

We select WFC3 calibration program 11928 (PI: Kozhurina-Platais) as our target dataset. Program 11928 comprises 9 visits with 15 exposures each, all targeting the center of globular cluster ω Centauri (NGC 5139). Each visit contains five filters (F098M, F110W, F125W, F139M, and F160W) at three dither positions, with dither offsets of approximately (0, 251) and (256, 251) pixels. For the sake of simplicity we use only two dither positions in each visit; it does not matter which two, as long as the offset between them is in only one direction (i.e. we select only (0,0) and (0, 251), or (0, 251) and (256, 251), but not (0,0) and (256, 251)). See Figure 1 for maps of observation coverage for all selected data.

We perform PSF photometry on the selected _flt frames of all visits using the WFC3 module of the photometry package DOLPHOT 2.0, a modified version of HSTphot (Dolphin 2000), using the recommended WFC3/IR parameters and PSFs[1]. DOLPHOT aligns all input images to a selected reference image and returns photometric information for all images in the coordinates of the reference image. This allows us to easily compare the magnitudes of stars that fall within a blob in the reference frame to their magnitudes when they fall outside a blob in the offset frame.

[1]See Appendix 1 for a full list of our DOLPHOT input parameters, Dolphin (2013a) for detailed descriptions of all parameters, and Dolphin (2013b) for recommendations for WFC3 photometry.

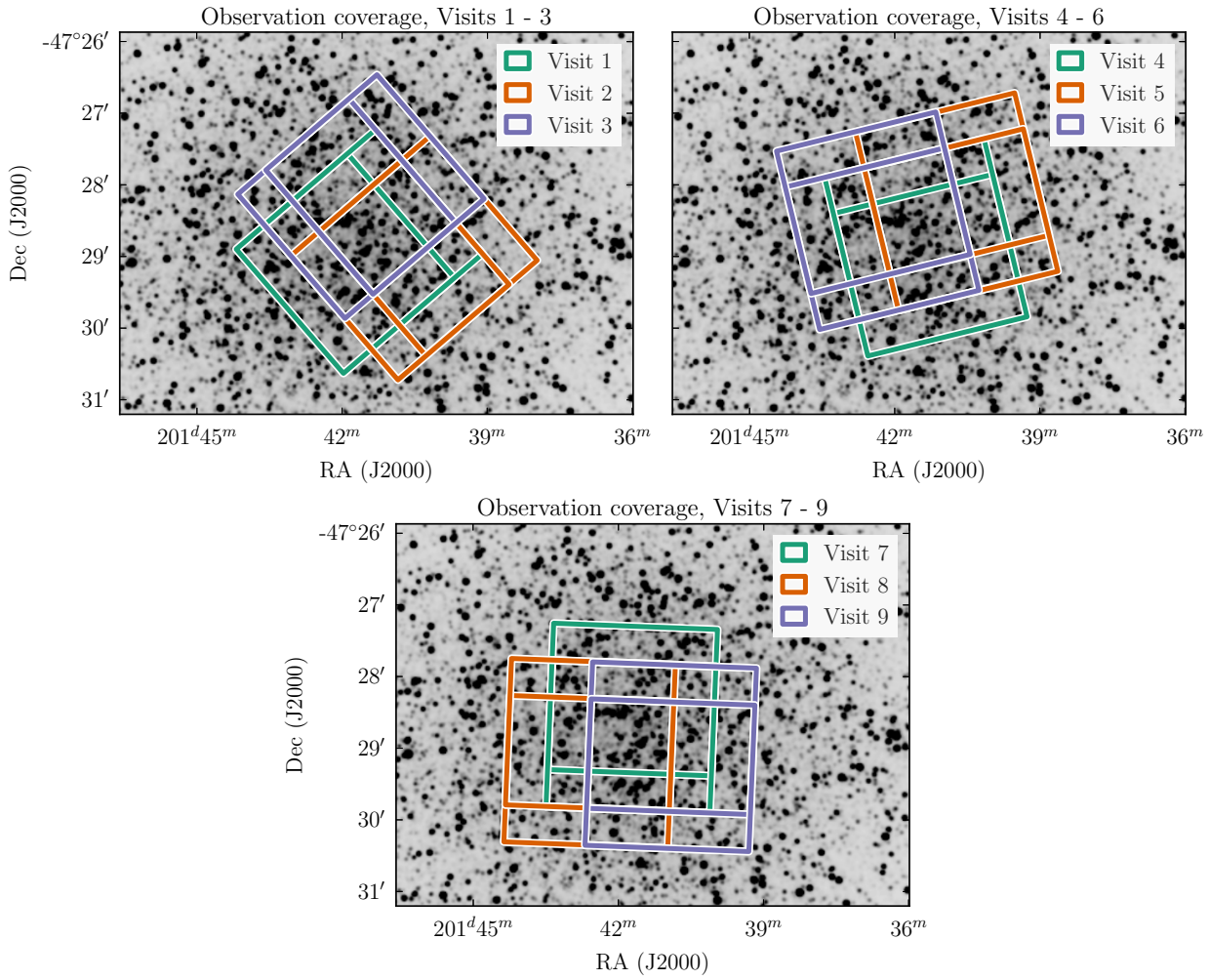

Figure 1: Instrument footprint maps for all images used for blob photometry. The background image used here is a J-band image from the Two Micron All Sky Survey (2MASS) (Skrutskie, M. F. et al. 2006).

From the complete DOLPHOT photometry catalog, we select the subset of stars that are at or above the 80th percentile in signal-to-noise and at or below the 10th percentile in crowding[2] in every filter for analysis, to ensure that any magnitude differences we find between images are primarily due to blobs and not other factors. We use percentile values for each filter because typical signal-to-noise and crowding values differ between filters, particularly between medium and wide-band filters.

[2]DOLPHOT's crowding parameter is defined as "how much brighter the star would have been [in magnitudes] measured had nearby stars not been fit simultaneously" (Dolphin 2013a).

Filter	SNR Cutoff	Crowding Cutoff
F098M	432.8	0.147
F110W	576.3	0.166
F125W	482.0	0.184
F139M	282.6	0.211
F160W	383.1	0.244

Table 1: Values for signal-to-noise ratio and crowding cutoffs for all filters.

After applying these selection criteria, we obtain a catalog of 53,471 stars across all visits. Many of these are likely to be repeated measurements of the same star (see Figure 1), but since we are characterizing an artifact on the detector rather than in space, all measurements are useful regardless of what stars they are performed on.

Out of these, we find a total of 284 stars that fall within one of 34 blobs in the reference frame, using the blob center coordinates and radii provided by M14. (We note that this means that under 1% of stars fall within a blob, as expected given that blobs affect only 1% of pixels; this alone indicates that blobs are not a large concern for typical observations of a resolved stellar field.) We assume that if a star falls within a blob in the reference frame coordinates, it will not fall within a different blob in the offset frame.

We then divide the original _flt frames by the blob flat field described by M14, creating new blob-flat-fielded images with extension _blt, and repeat the photometry process described above with all the same parameters, which enables us to isolate and evaluate the effects of the blob flat field on stellar photometry. Out of this new set of photometry, we find 277 stars that correspond to the stars found within blobs in the original photometry, or a 97.5% recovery rate.

To quantify how the blobs affect stars, we measure the attenuation factor $A_{\rm blob}$ experienced by each star. The "attenuation factor" as used here is a semi-arbitrary measure of the attenuation the star experiences due to the blob, defined as the sum of the pixel values in the blob flat field within a 3-pixel aperture radius at the location of the star, where unity has been subtracted from the original blob flat field to better indicate the level of attenuation relative to nonaffected regions; thus, an attenuation factor of 0 indicates that the star experiences no attenuation, whereas an attenuation factor of -3 indicates that the star experiences $\sim$10% attenuation on all the pixels it falls on.

In Figures 2 and 3 we plot the difference in a star's magnitude outside a blob minus the same star's magnitude when it falls within a blob; the differences between images with and without the blob flat field applied are apparent.

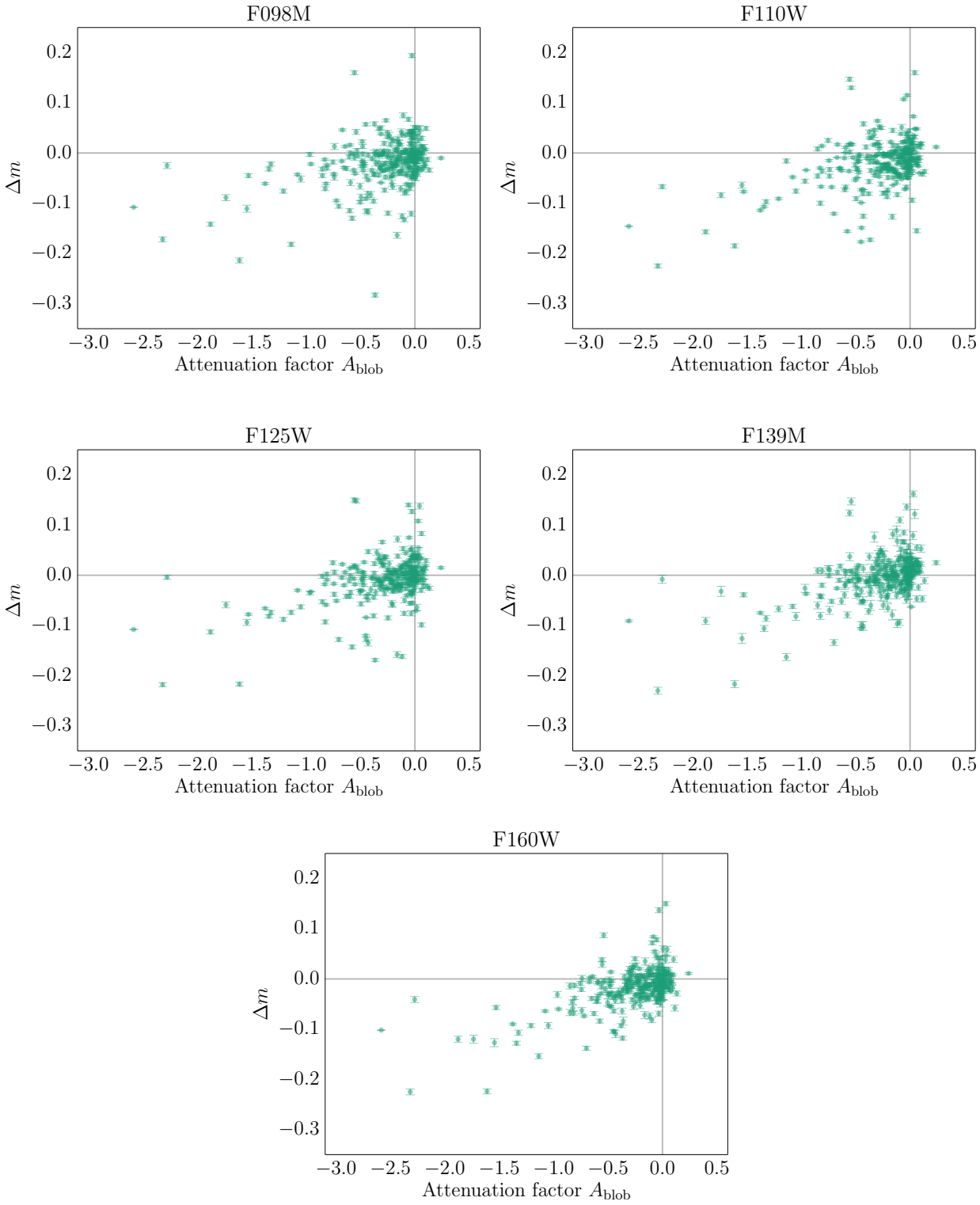

Figure 2: Difference in stellar magnitude outside minus inside a blob for images without the blob flat field applied.

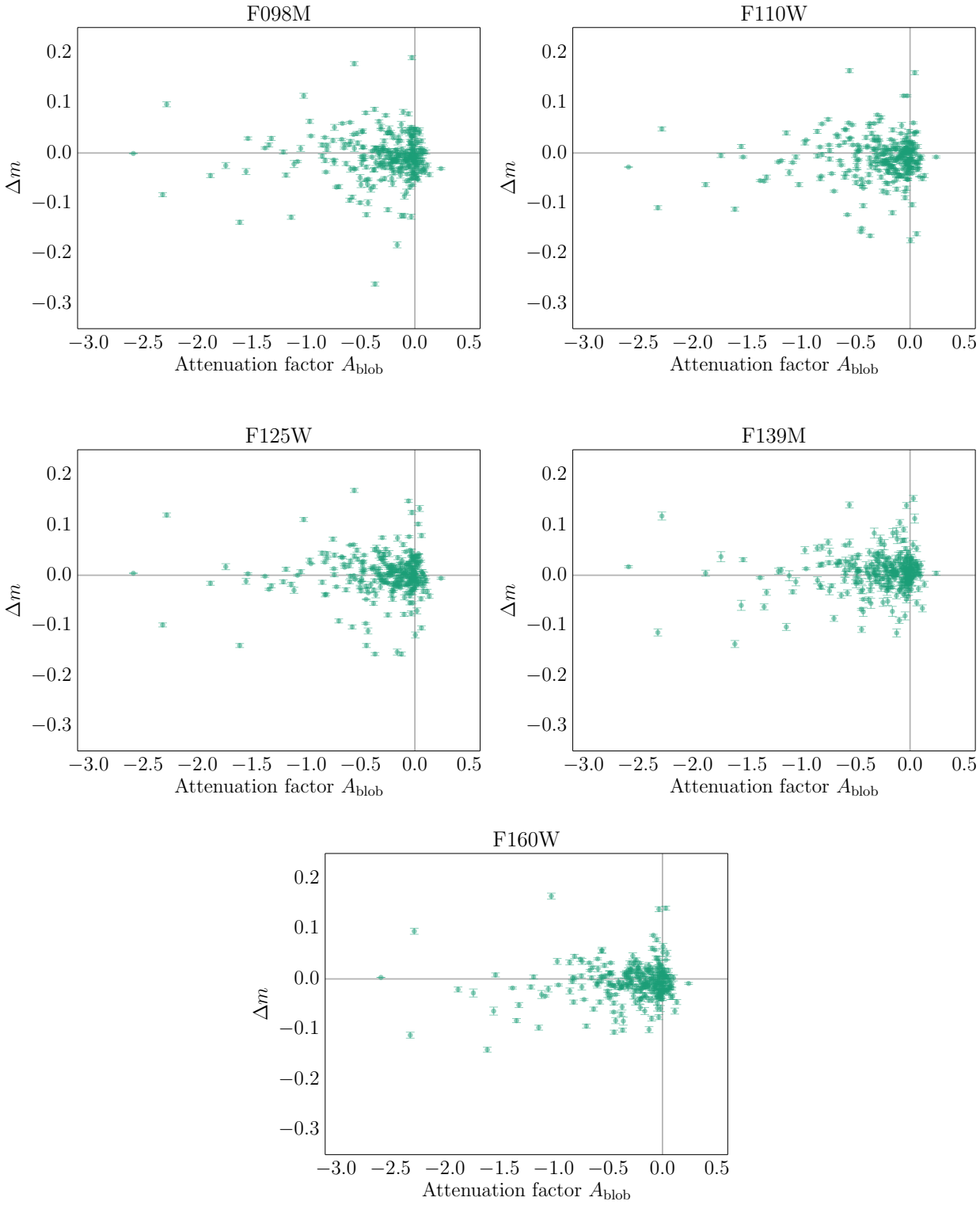

Figure 3: Difference in stellar magnitude inside vs. outside a blob for images with the blob flat field applied, using the same measure of "attenuation factor" as previously defined. The correlation of Δm with attenuation factor is no longer apparent, as it was in Figure 2.

It is possible to estimate analytically the amount of flux that a blob absorbs from a star, and the corresponding flux that the blob flat can correct for. For a star of blob-affected flux $f_{\star,\mathrm{orig}}$ affected by a blob region of attenuation A_{blob} within aperture radius R, the corrected flux $f_{\star,\mathrm{corr}}$ will be:

$$f_{\star,\mathrm{corr}} = \frac{f_{\star,\mathrm{orig}}}{(A_{\mathrm{blob}}/\pi R^2) + 1} \tag{1}$$

If we convert this to magnitudes, we can find the magnitude Δm_{corr} that the blob flat reintroduces to an attenuated star:

$$m_{\star,\mathrm{corr}} = -2.5 \log_{10} \left(\frac{f_{\star,\mathrm{orig}}}{(A_{\mathrm{blob}}/\pi R^2) + 1} \right) \tag{2}$$

$$= m_{\star,\mathrm{orig}} + 2.5 \log_{10} \left(\frac{A_{\mathrm{blob}}}{\pi R^2} + 1 \right) \tag{3}$$

$$\Delta m_{\mathrm{corr}} = 2.5 \log_{10} \left(\frac{A_{\mathrm{blob}}}{\pi R^2} + 1 \right) \tag{4}$$

$$\approx 1.0857 \left(\frac{A_{\mathrm{blob}}}{\pi R^2} - \frac{1}{2} \left(\frac{A_{\mathrm{blob}}}{\pi R^2} \right)^2 \right) \tag{5}$$

This relation assumes uniform blob attenuation over the aperture area, and does not take into account PSF weighting, but is nevertheless a useful heuristic for evaluating against the empirical changes we find in our photometry. When we compare equation 4 to the empirical Δm_{corr} values from our photometry, as shown in Figure 4, we find that the empirical slope of Δm_{corr} is slightly steeper than predicted, likely due to the weighting of the central pixel in the PSF fitting. It is probable that most if not all of the scatter in the empirical Δm_{corr} values can be explained by nonuniformities in the blob flat field and the weighting of the stellar PSF. Equation 5 is the second-order Taylor series approximation to equation 4.

One possible concern is that blobs may affect stellar photometry indirectly by affecting the sky values surrounding a star. While this may indeed be a factor for low signal-to-noise stars or stellar sources in the presence of bright, extended emission, for this work it is not an issue; we find that for stars that are at or above the 80th percentile in signal-to-noise and at or below the 10th percentile in crowding, the ratio of the sky values to the counts inside the photometry aperture as calculated by DOLPHOT has a median of about 0.5%, and is about 3% in the worst case; thus, for our purposes we can disregard any effect the blob may have on the surrounding sky.

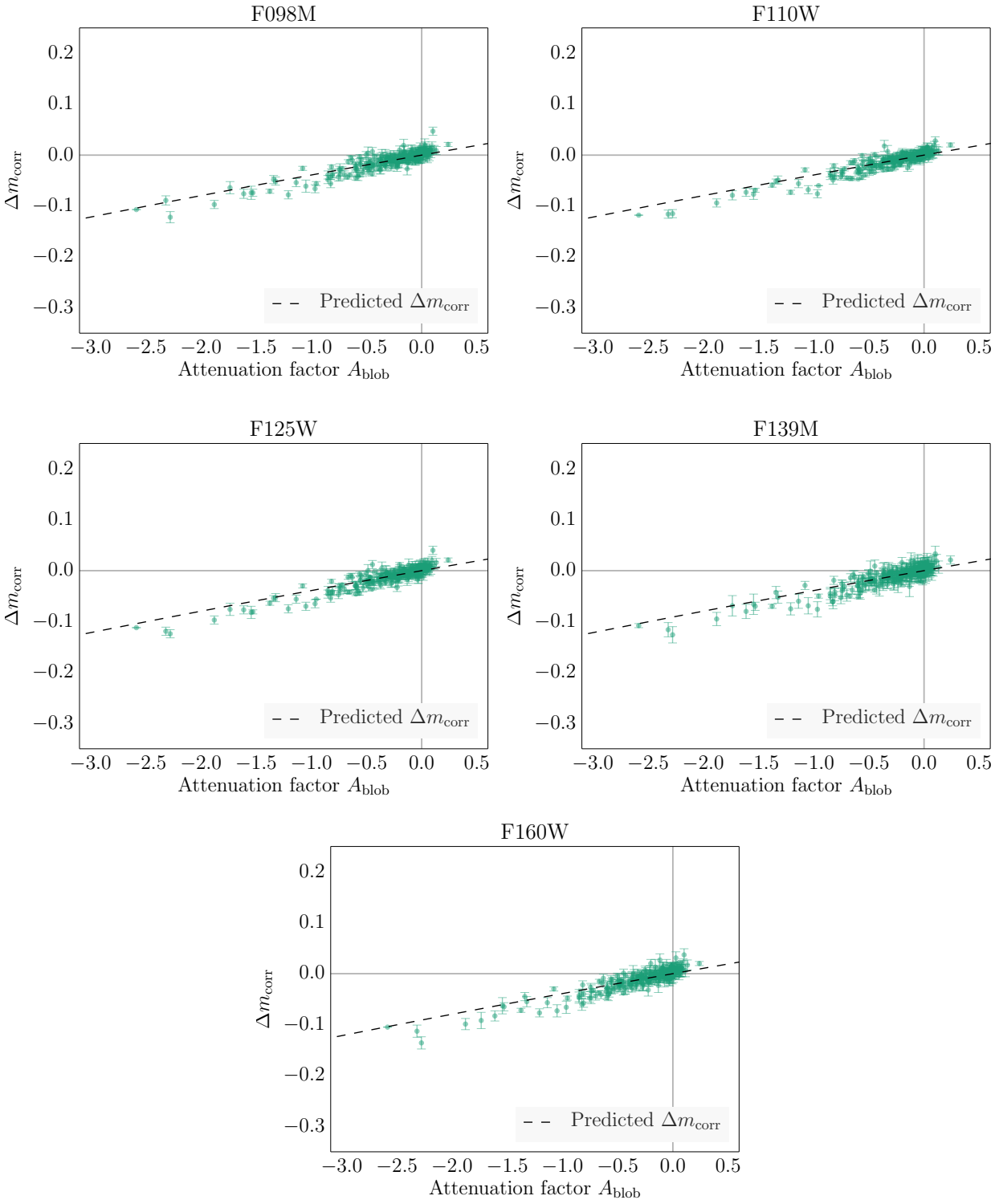

Figure 4: The amount of magnitude reintroduced to blob-affected stars by the blob flat field; the stronger the blob attenuation, the more negative the change in stellar magnitude when the blob flat is applied. For the stars that experience the most attenuation, they are measured to be $\sim$0.12 mag brighter when the blob flat field is applied.

The plots in Appendix 1 depict the locations of stars on blobs, and in many of the blobs there appear to be overdensities of stars near the edges and underdensities near the centers, where blob attenuation is greatest. It may be possible that the blobs are causing stars to be erroneously rejected from the photometry catalog, either due to low signal-to-noise, or sharpness or roundness being affected by steep attenuation gradients. To assess whether this is truly the case, we create a histogram of the distances of stars from the blob centers (divided by the blob radius for each blob, as blobs have different radii), and compare that to the predicted number of stars in each radial bin assuming a uniform surface density of stars over all blobs, as shown in Figure 5.

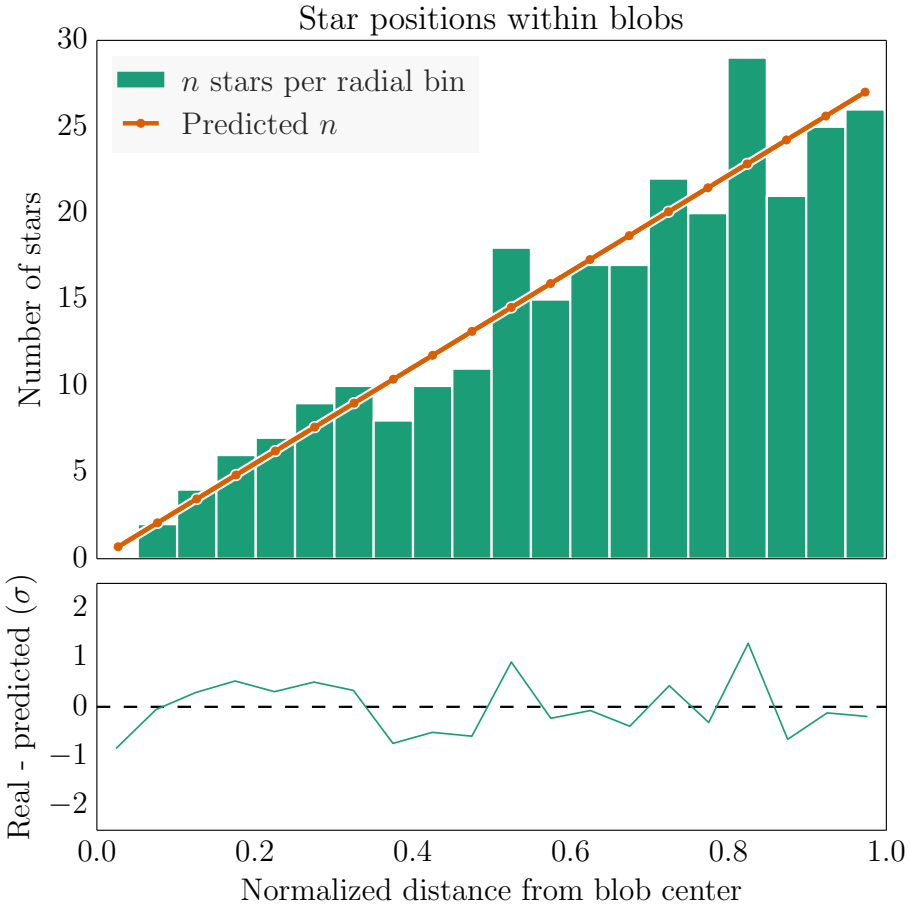

Figure 5: Histogram of the radial distribution of stars within blobs., and their deviation from values predicted from a uniform stellar surface density, where $\sigma = \sqrt{n}$. There is only one radial bin where the deviation from the predicted value exceeds $+1\sigma$, and none where it exceeds -1σ.

Based on Figure 5, we find no evidence that blobs prevent stars from being found by DOLPHOT altogether nearer to their centers.

We also evaluate the changes in stellar signal-to-noise, roundness, and sharpness on flat-fielded vs. non-flat-fielded images (Figure 6).

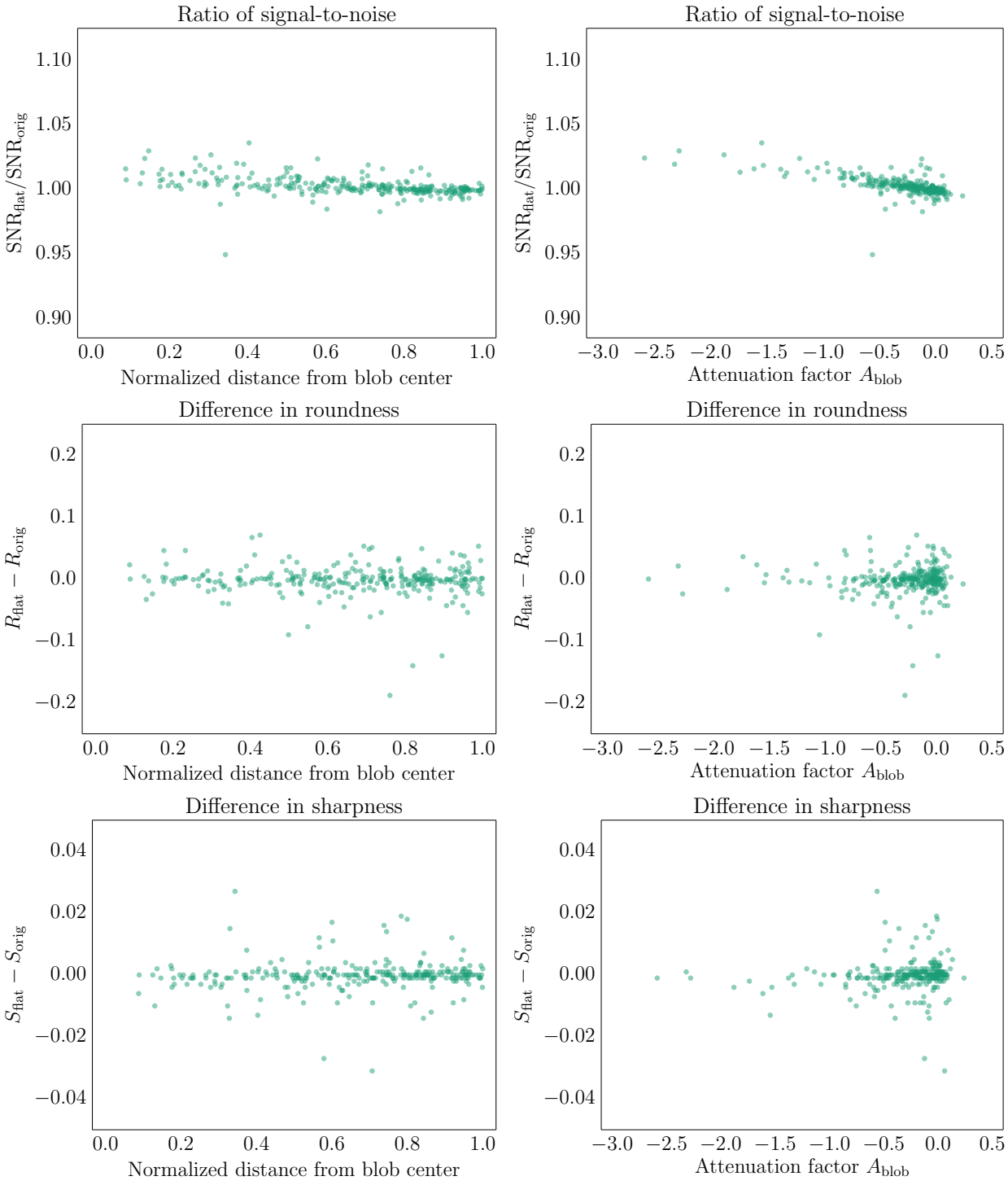

Figure 6: Overall signal-to-noise, roundness R, and sharpness S, compared between flat-fielded and non-flat-fielded images. We find a slight systematic improvement in the analytically estimated signal-to-noise ratio with application of the blob flat field, as expected due to the removal of attenuation by the flat field, but no evidence of systematic changes in analytically estimated roundness or sharpness. We also note that the signal-to-noise ratios are all between 0.95 and 1.05; thus, the blobs are only a concern for photometry at the 5% or better precision level.

We also notice that the values of Δm in Figure 2 appear to be biased slightly for each filter relative to another filter. For example, in Figure 2, the data points for F139M can be seen by visual inspection to be on average slightly greater than those for F160W. These differences appear in both Figure 2 or Figure 3; the blob flat has little to no effect on them, which could indicate a wavelength dependency of the attenuation of the blobs. In Tables 2 and 3 we provide the median of differences of the stellar photometry in one filter to another. We conclude that the blob attenuation is approximately achromatic because the maximum absolute value in Tables 2 and 3 is 0.017 mag, i.e. less than 2% photometric difference.

	F098M	F110W	F125W	F139M	F160W
F098M	0.000	0.003	−0.009	−0.016	0.000
F110W	−0.003	0.000	−0.011	−0.017	−0.003
F125W	0.009	0.011	0.000	−0.007	0.009
F139M	0.016	0.017	0.007	0.000	0.012
F160W	0.000	0.003	−0.009	−0.012	0.000

Table 2: Median of differences in Δm illustrated in Figure 2.

	F098M	F110W	F125W	F139M	F160W
F098M	0.000	0.002	−0.011	−0.016	0.000
F110W	−0.002	0.000	−0.011	−0.016	−0.000
F125W	0.011	0.011	0.000	−0.006	0.008
F139M	0.016	0.016	0.006	0.000	0.013
F160W	0.000	0.000	−0.008	−0.013	0.000

Table 3: Median of differences in Δm illustrated in Figure 3.

As a final check of the quality of photometry for blob-affected stars with the flat field applied, we examine stellar magnitude vs. Δm for both blob-affected stars and all stars in our dataset that meet the specified SNR and crowding criteria, as shown in Figure 7. We also show predicted Δm values at the 1 and 2σ levels based on the signal-to-noise estimates DOLPHOT provides, where $\sigma = \sqrt{2/\mathrm{SNR}}$. We find that in all filters over 73% of blob-affected stars have Δm within 1σ, and over 92% are within 2σ. Percentages for all filters are shown in Table 4. From this we conclude that the photometry of blob-affected stars with the flat field applied is comparable to photometry of stars that are unaffected by blobs.

Filter	% within 1σ	% within 2σ
F098M	77.4	94.0
F110W	73.9	92.2
F125W	82.3	92.6
F139M	88.3	97.2
F160W	86.6	96.8

Table 4: Fraction of flat-fielded blob stars with Δm within 1 and 2σ of the predicted Δm.

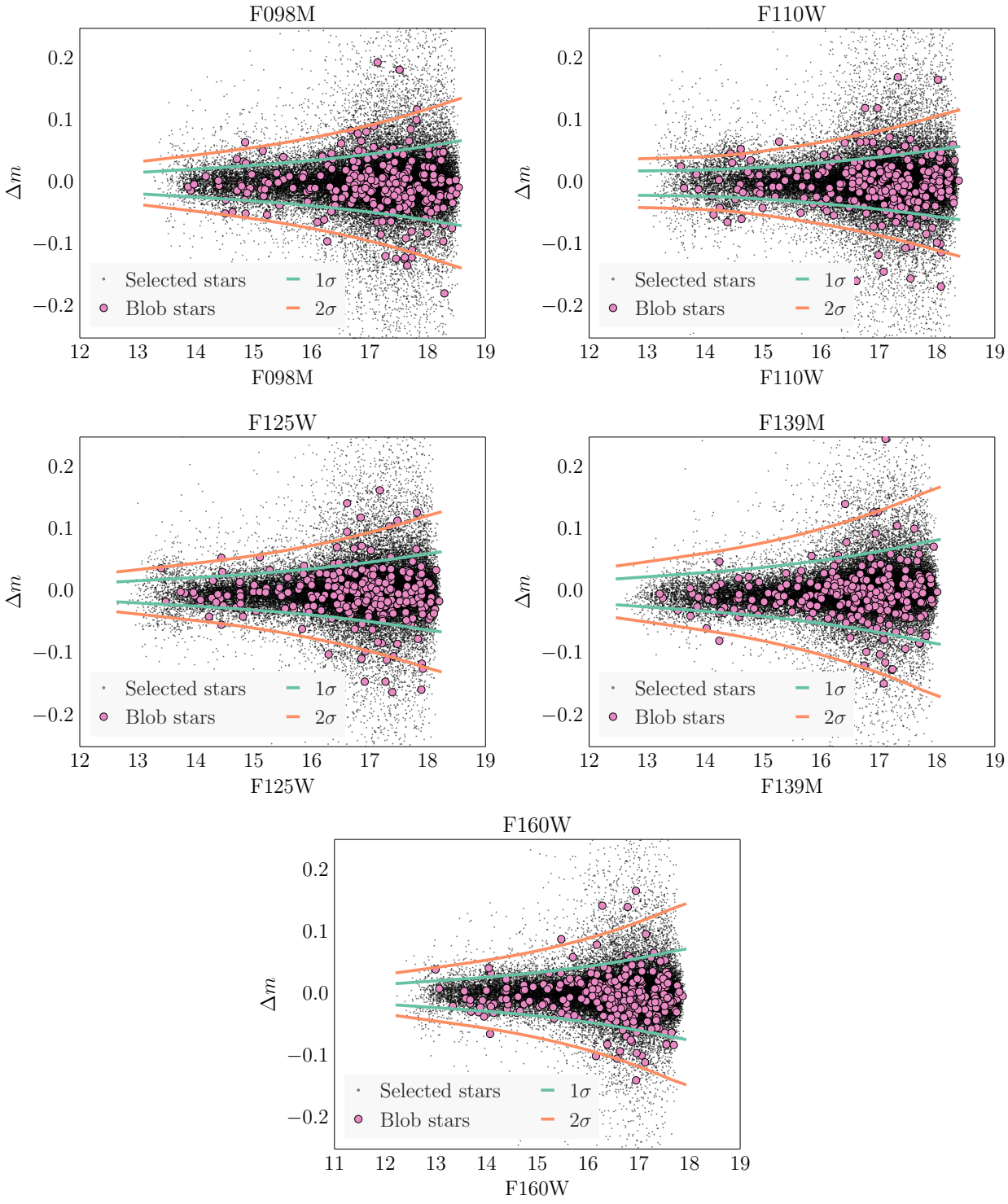

Figure 7: Magnitude vs. Δm for both blob-affected stars and all high-SNR/low-crowding stars, as well as estimates for 1 and 2σ deviations from zero for Δm. We note that the spread in Δm appears to get markedly larger at the brightest magnitudes in some filters; this is due to saturation. For example, for F125W 70% of the saturation limit is reached within the sampling time (2.932 seconds) at approximately 13.5 mag, and 14.3 mag for F110W, which is where we begin to see marked changes in the spread of Δm for both filters.

Conclusions

Based on DOLPHOT photometry of globular cluster ω Centauri, we have demonstrated that the application of the blob flat field improves photometry for stars in blob-affected regions of the WFC3 IR detector. The correction to magnitudes in these regions can be as large as 0.1 mag, and the quality of the photometry on flat-fielded stars is comparable to that of stars that are unaffected by blobs. M14's reservations about using the blob flat fields seem to have been unfounded. However, we note that most observations will not be significantly affected by blobs, as blobs occupy only 1% of the detector area and their effects can be mitigated by dithering and drizzling. The use of the blob flat to improve stellar photometry is most effective in crowded fields where there has been no dithering or where stellar photometry is performed on individual exposures.

Acknowledgements

We would like to thank Knox Long for his insights during the review process, and Kyle Van Gorkom for his assistance with DOLPHOT. This research made use of Astropy, a community-developed core Python package for astronomy (Astropy Collaboration et al., 2013).

References

Astropy Collaboration, T. P. Robitaille, E. J. Tollerud, P. Greenfield, M. Droettboom, E. Bray, T. Aldcroft, M. Davis, A. Ginsburg, A. M. Price-Whelan, W. E. Kerzendorf, A. Conley, N. Crighton, K. Barbary, D. Muna, H. Ferguson, F. Grollier, M. M. Parikh, P. H. Nair, H. M. Unther, C. Deil, J. Woillez, S. Conseil, R. Kramer, J. E. H. Turner, L. Singer, R. Fox, B. A. Weaver, V. Zabalza, Z. I. Edwards, K. Azalee Bostroem, D. J. Burke, A. R. Casey, S. M. Crawford, N. Dencheva, J. Ely, T. Jenness, K. Labrie, P. L. Lim, F. Pierfederici, A. Pontzen, A. Ptak, B. Refsdal, M. Servillat, and O. Streicher. Astropy: A community Python package for astronomy. AAP, 558:A33, October 2013. doi: 10.1051/0004-6361/201322068.

Dolphin, A. E., 2013a, DOLPHOT User's Guide, version 2.0

Dolphin, A. E., 2013b, DOLPHOT/WFC3 User's Guide, version 2.0

Dolphin, A. E., 2000, WFPC2 Stellar Photometry with HSTphot, PASP, 112, 1383

McCullough, P. R., Mack, J., Dulude, M., & Hilbert, B. 2014, Infrared Blobs: Time-dependent Flags, ISR WFC3 2014-21

Pirzkal, N. & Hilbert, B. 2012, The WFC3 IR "Blobs" Monitoring, ISR WFC3 2012-15

Pirzkal, N., Viana, A., & Rajan, A. 2010, The WFC3 IR "Blobs," ISR WFC3 2010-06

Skrutskie, M. F., et al. 2012, The Two Micron All Sky Survey (2MASS), AJ, 131, 1163

Appendix 1: DOLPHOT Parameters

```
Nimg = 10                    # photometry done by visit; 10 images per visit
img0_file = ibcj01tmq_flt    # coordinate reference image
img1_file = ibcj01tmq_flt
img2_file = ibcj01tvq_flt
img3_file = ibcj01toq_flt
img4_file = ibcj01u1q_flt
img5_file = ibcj01trq_flt
img6_file = ibcj01tzq_flt
img7_file = ibcj01tpq_flt
img8_file = ibcj01txq_flt
img9_file = ibcj01ttq_flt
img10_file = ibcj01u3q_flt
img_RAper = 3        # photometry aperture for each image (pixels)
img_apsky = 8 20     # sky annulus for aperture correction (pixels)
img_RSky = 8 20      # inner and outer radius for sky value calc (pixels)
img_RChi = 1.5
img_RPSF = 10        # PSF radius (pixels)
SkipSky = 1
SkySig = 2.25
SigFind = 8          # sigma threshold for star detection
SigFinal = 20        # sigma threshold for star to be included in final output
SigFindMult = 0.85
MaxIT = 25
NoiseMult = 0.10
FSat = 0.999
ApCor = 1            # perform aperture correction? 1 = yes
RCentroid = 2
PosStep = 0.25
RCombine = 1.5
SigPSF = 10.0
PSFres = 1           # solve for PSF residuals? 1 = yes
PSFPhot = 1          # type of photometry; 1 = standard PSF-fitting
PSFPhotIt = 3        # number of iterations in PSF-fitting photometry
FitSky = 1
Force1 = 1           # force all detections to be type 1 (bright star)
Align = 4            # full alignment solution
AlignIter = 5
Rotate = 1
SecondPass = 5       # find faint stars in wings of brighter stars
UseWCS = 1
FlagMask = 4         # error flags to reject on; 4 = saturation
WFC3IRpsfType = 0    # use Anderson PSF cores?
InterpPSFlib = 1     # interpolate PSFs based on position on detector
```

Appendix 2: Blob Maps

For each blob, we overplot apertures representing all stars found within that blob on the blob flat field. Here red is positive divergence from unity and blue is negative. The blob identification numbers and coordinates are as listed by M14.

Blob 2 (106.9, 868.2)

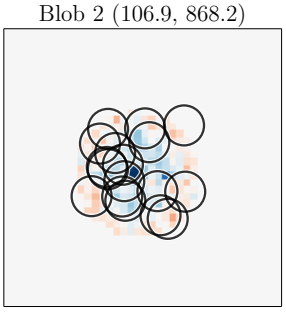

Blob 3 (134.1, 971.5)

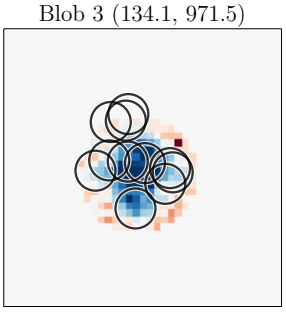

Blob 4 (171.3, 976.3)

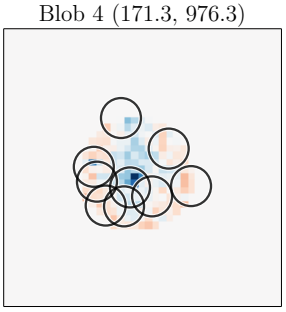

Blob 5 (235.8, 423.1)

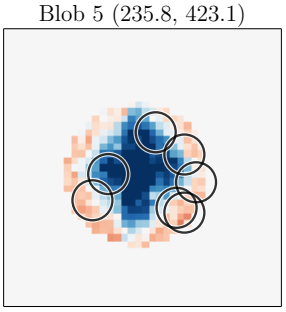

Blob 9 (324.6, 393.4)

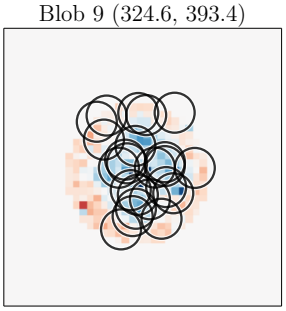

Blob 10 (326.9, 1000.1)

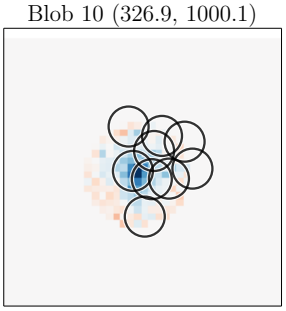

Blob 11 (358.1, 762.8)

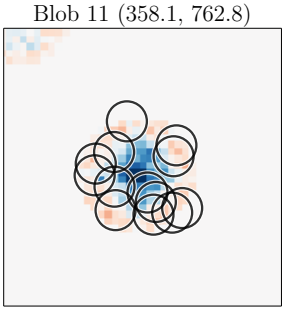

Blob 12 (413.0, 89.0)

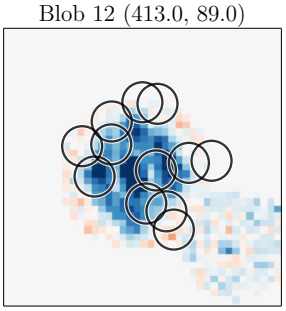

Blob 14 (442.8, 924.7)

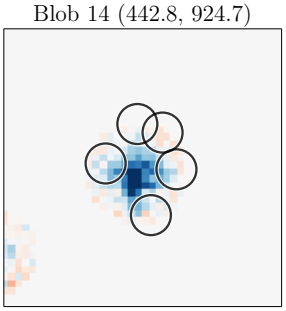

Blob 15 (474.3, 380.4)

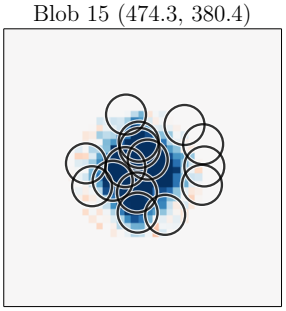

Blob 17 (588.1, 883.1)

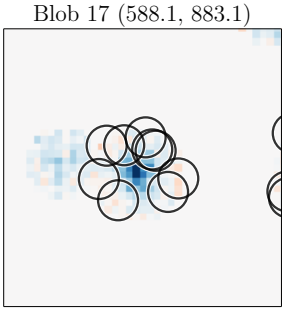

Blob 18 (611.8, 617.2)

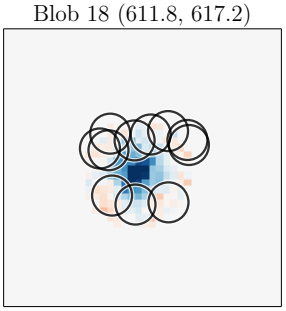

Blob 19 (614.0, 883.2)

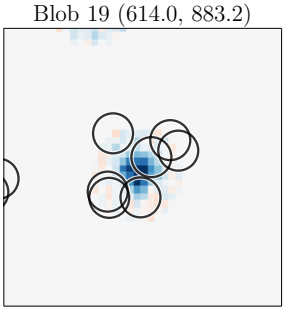

Blob 20 (681.1, 908.2)

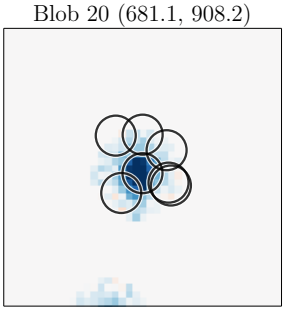

Blob 21 (719.0, 645.0)

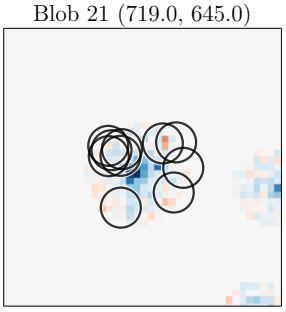

Blob 23 (827.9, 673.2)

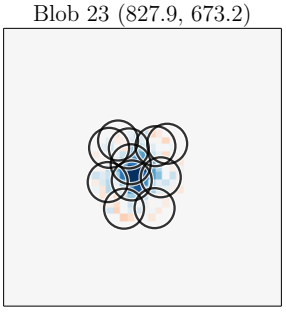

Blob 24 (868.0, 839.2)

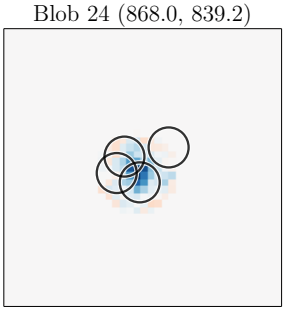

Blob 25 (884.1, 334.2)

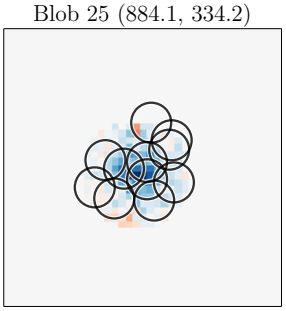

Blob 26 (970.6, 147.8)

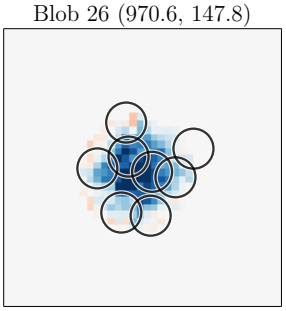

Blob 27 (974.0, 579.1)

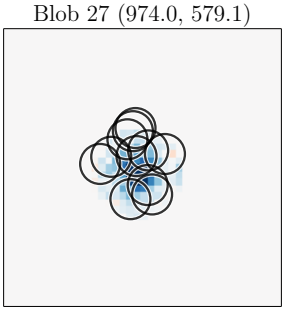

Blob 29 (30.0, 227.0)

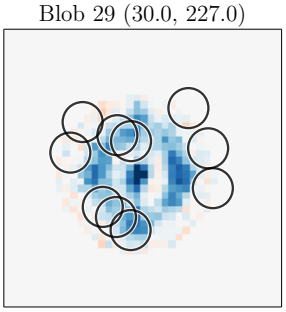

Blob 30 (52.0, 13.0)

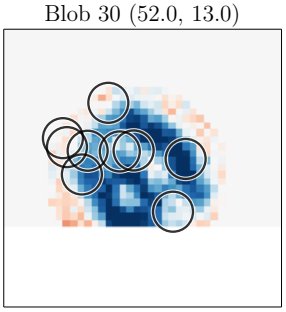

Blob 32 (308.0, 52.0)

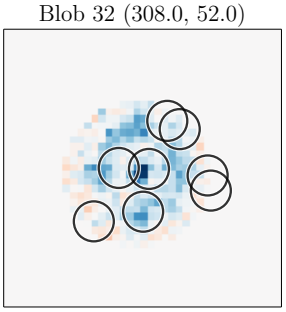

Blob 33 (406.0, 706.0)

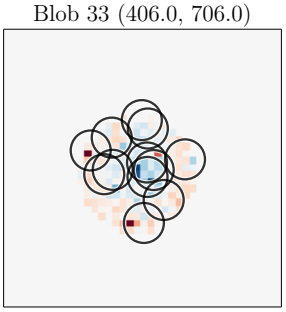

Blob 34 (561.1, 793.2)

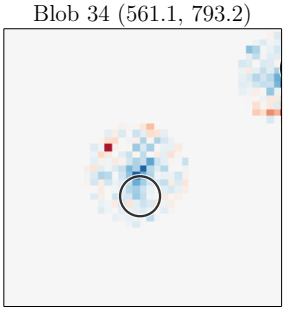

Blob 35 (571.7, 833.2)

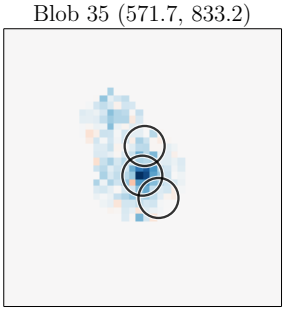

Blob 36 (582.1, 807.0)

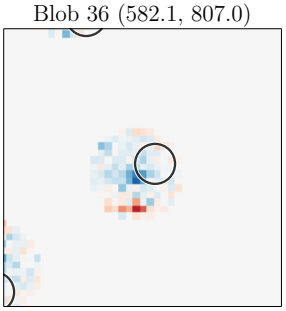

Blob 38 (800.9, 496.0)

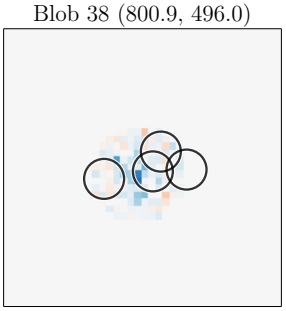

Blob 39 (821.0, 629.2)

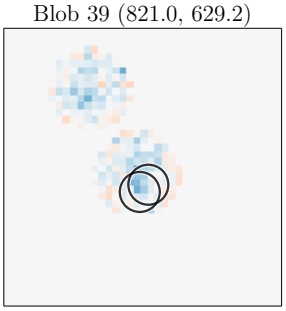

Blob 40 (824.6, 584.9)

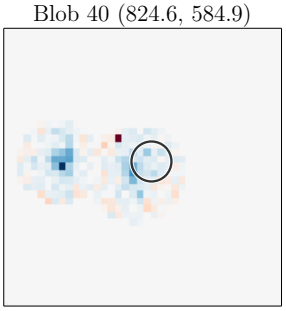

Blob 41 (827.3, 922.8)

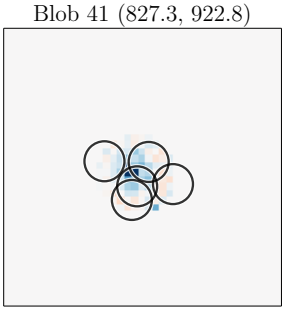

Blob 42 (869.6, 42.7)

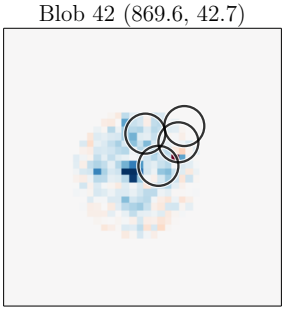

Blob 44 (973.0, 637.0)

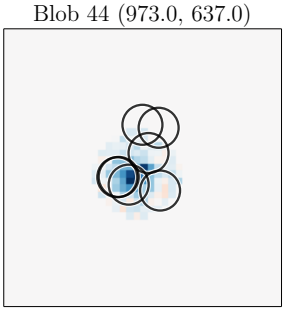

Blob 45 (1006.0, 599.0)